Composition, size distribution, optical properties and radiative effects of laboratory resuspended PM_{10} from geological dust of Rome area, by electron microscopy and radiative transfer modelling

A. Pietrodangelo,[1] R. Salzano,[1] C. Bassani,[1] S. Pareti,[1] and C. Perrino[1]

(1){ Institute of Atmospheric Pollution Research, National Research Council, Italy }

Correspondence to: A. Pietrodangelo (pietrodangelo@iia.cnr.it)

Abstract

In this work, new information has been gained on the laboratory resuspended PM_{10} fraction from geological topsoil and outcropped rocks representative of Rome area, Latium.

Mineralogical composition, size distribution, optical properties and the surface radiative forcing efficiency (RFE) of dust types representing the compositional end-members of this geological area have been addressed. A multi-disciplinary approach was used, based on chamber resuspension of raw materials and sampling of the PM_{10} fraction, to simulate field sampling at dust source, scanning electron microscopy / X-ray energy-dispersive microanalysis (SEM XEDS) of individual mineral particles, X-ray diffraction (XRD) analysis of bulk dust samples, building of number and volume size distribution (SD) from microanalysis data of mineral particles and fitting to Log-normal curve, and radiative transfer modelling (RTM) to retrieve optical properties and radiative effects of the compositional end-member dust samples.

The mineralogical composition of Rome lithogenic PM_{10} varies between an end-member dominated by silicate minerals (from volcanics lithotypes), and one mostly composed of calcite (from travertine or limestones). Lithogenic PM_{10} with intermediate composition derives mainly from siliciclastic rocks or marlstones. Size and mineral species of PM_{10} particles of silicate-dominated dust types are tuned mainly by rock weathering and, to lesser extent, by debris formation or crystallization; chemical precipitation of $CaCO_3$ plays a major role in calcite-dominated types. These differences reflect in the diversity of volume distributions, either within dust types, or mineral species. Differences are also observed between volume distributions of calcite from travertine (natural source; SD unimodal at 5 µm a.d.) and from road dust (anthropic source; SD bimodal at 3.8 and 1.8 µm a.d.). The volcanics and travertine dusts affect differently the single scattering albedo (SSA) and the asymmetry parameter (g) in the VISible and Near Infrared (NIR) regions. The downward component of the Bottom Of Atmosphere (BOA) solar irradiance simulated by RTM for an atmosphere where only volcanics, or only travertine dust, composes the aerosol, shows that volcanics contribution to the solar irradiance differs significantly from that of travertine in the NIR region, while similar contributions are modelled in the VIS. The RFE (293 W/m^2 for volcanics and 139 W/m^2 for travertine, at 50° solar zenith angle) shows that volcanics dust produces a stronger cooling effect at surface than travertine, as expected for more absorbing aerosols.

1 Introduction

Airborne geological dust sourced from topsoil and surface rocks critically contribute to the total mass, composition, microphysical and optical properties of the atmospheric aerosol in continental regions, and largely impacts different Earthôs compartments by transport and deposition (Scheuvens and Kandler, 2014). Crustal particles commonly constitute the major mass fraction of the re-suspended lithogenic materials and influence significantly both the PM mass concentration at ground (Perrino et al., 2009; Viana et al., 2014) and the mineral composition. The latter varies mostly depending both on the rock types outcropping in the source region (Dürr et al., 2005; Journet et al., 2014) and, consequently, on the crystallization, sedimentation and weathering processes tuning the particle size and shape (Claquin et al., 1999). This has been observed for mineral dust of African desert regions (Caquineau et al., 2002; Evans et al., 2004; Stuut et al., 2009; Scheuvens et al., 2013; Formenti et al., 2014) and of arid areas in other regions (Kim et al., 2006; Jeong, 2008; Moreno et al., 2009; Agnihotri et al., 2013; Rashki et al., 2013). Either microphysical (size distribution and complex refractive index) and optical properties of airborne lithogenic dust vary as a consequence of the mineralogical composition (Sokolik and Toon, 1999; Reid et al., 2003; Hansell et al., 2011; Wagner et al., 2012; Di Biagio et al., 2014; Mahowald et al., 2014; Smith and Grainger, 2014). When at a certain site intrusions of lithogenic dust at ground occur, like desert dust, the overall properties of the PM may be altered, compared to periods when this contribution is negligible (Meloni et al., 2006; Choobari et al., 2014). This also affects the impact of airborne aerosol on the energy balance of the Earth ï solar system. Airborne lithogenic dust plays a role both in the direct mechanisms (light scattering and absorption) and in the indirect mechanisms (cloud-aerosol interactions) which tune the Earthôs radiative budget (Sokolik et al., 2001; Choobari et al., 2014). While indirect effects depend on the heterogeneous chemistry occurring at particles surface (Levin et al., 1996; Buseck and Pósfai, 1999; Sokolik et al., 2001; Krueger at al., 2004; Kandler et al., 2007), the light scattering and absorption are mostly controlled by the mineralogical composition, shape features and microphysical properties of geological particles ((DôAlmeida, 1987; Kalashnikova and Sokolik, 2002 and 2004; Kokhanovsky, 2008; Hansell et al., 2011).

Most studies facing this issue relate to desert dust from Sahara and Sahel regions (Kandler et al., 2007 and 2009; Müller et al., 2009; Papayannis et al., 2012; Wagner et al., 2012; Di

Biagio et al., 2014). Nevertheless, knowledge gaps still exist on this issue (Rodríguez et al., 2012), due to the site-related large variability of dust mineralogical features (elemental and mineral composition, crystalline structure, shape, microphysical and optical properties).

Also, only few of the published studies characterize the re-suspended geological dust of non-African regions (Falkovich et al., 2001; Peng and Effler, 2007; Rocha-Lima et al., 2014). Large areas of Italy, especially those closer to the Mediterranean Basin, are affected by dryness, heavy anthropic impact (urbanization, farming, quarry activities, etc.), erosion and poor vegetation cover, leading to increased desertification risk. The National Atlas of areas under risk of desertification of Italy reports, for instance, that the yearly average of dry soil days in the region of Latium ranges 64 ÷ 110 (Costantini et al., 2007 and 2009). In Fig. 1S this is showed for the area of study of this work; the highest number of dry soil days (86 ÷ 110) is found in the northern zone of the study area (Geoportale Nazionale, 2011). Latium is also characterised by a large surface where poorly-developed soils and debris deposits are present, which are easily affected by massive erosion.

Consequently, the resuspension of mineral dust from local lithological domains contributes notably to the ambient PM_{10} of Rome area. This is shown in Figures 2S and 3S for the Villa Ada site (Rome, urban background) and the Montelibretti EMEP site (Rome outskirts, rural background), respectively. Considering the 2005 ï 2011 period, among days which show a dominant (over 50% of total PM_{10} mass) crustal contribution to the ambient PM_{10} composition at these sites, desert dust intrusions at-ground (DD-days) account for 60% at Montelibretti and 30% at Villa Ada, while the remaining days are reasonably affected by local crustal contributions, given the background character of the considered sites (LD-days). Interestingly, among the above described days, the mass concentration of the crustal matter on LD-days is in many cases comparable with that observed on DD-days. Within this picture, main goals of this work were: to study the relationships between the local outcropped rocks (or topsoil) and the dust particles in the PM_{10} sourced from these rocks, and to gain knowledge about the microphysical and optical properties of the mineral PM_{10} at geological dust source, and on the downward radiative flux at BOA (Bottom Of Atmosphere) related to an atmosphere where the only aerosol component is the PM_{10} dust, in order to define the radiative effects which are due to the local mineral dust only In a previous study, we determined elemental source profiles of the PM_{10} fraction of local mineral dust (Pietrodangelo et al., 2013). In this work, the PM_{10} fraction of the same samples was characterized with respect to the above goals. To investigate relationships among these different aspects, a multi-

faceted analysis was performed, on the basis of the following approaches: chamber resuspension of raw materials and PM10 sampling, to simulate field sampling at dust source, scanning electron microscopy / X-ray energy-dispersive microanalysis (SEM XEDS) of individual mineral particles, X-ray diffraction (XRD) analysis of bulk dust samples, number and volume size distribution (SD) building from microanalysis data of mineral particles and fitting to Log-normal curve, and radiative transfer modelling (RTM) to retrieve optical properties and radiative effects. Results from experimental and modelling analysis are discussed for their consistency with both the lithological nature of major local dust sources and the microphysical properties of the mineral dust samples.

2 Approach and methodology

2.1 Study area, dust collection and sample treatment

Mineral dust was collected from topsoil and debris of rural areas surrounding the city of Rome within a perimeter of 50 km radius. On the basis of criteria established after geological analysis of the Latium region, the following geodynamics domains were considered: the volcanic complexes, the marine (limestones, marlstones and sandstones) deposits, the siliciclastic series (mainly flysch) and the quaternary deposits (mainly travertines).

Sampling areas of about 4 km^2 were selected within each local geodynamics domain; a number of dust collection points was identified, within each area, to obtain sub-samples of raw material, from which the final samples were obtained. The number of sampling areas varies within each domain, depending on the geographical extension and the geological complexity of the domain. Furthermore, paved road dust was collected by brushing the surface of different roads within the volcanic and the travertine domains. PM_{10} dust was laboratory resuspended from the bulk rocks samples, and from road dust, by a resuspension chamber, and collected by low-volume sampling on polycarbonate membranes for SEM XEDS microanalysis. It is worth noting that, among laboratory methods of dust generation or resuspension from bulk materials, fluidization by mechanical ventilation in a resuspension chamber is widely acknowledged, either for not affecting both the complete resuspension potential of the source material and the original size distribution of the resuspended particles in the material itself, and for simulating the resuspension of dust previously deposited at a site (Gill et al., 2006 and references therein). By this approach, good approximation of the field

sampling at a dust source can be achieved, making it suitablefor studies on the mineralogical and microphysical characterization of mineral dust (Gill et al., 2006 and references therein; Feng et al., 2011; Aimar et al., 2012; Dobrzhinsky et al, 2012). The whole geological siting criteria, dust sampling strategy, laboratory treatment details and elemental profiles of the re-suspended dust types, are fully described in Pietrodangelo et al. (2013). In that paper we discussed how, under the perspective of mineral composition, the volcanics (silicate-dominated rocks) and the travertine (calcite-dominated rocks) can be considered as reference compositional end-members of the overall outcropping lithotypes in the Latium region (Cosentino et al., 2009), while the sedimentary domains (marine deposits and siliciclastic series) represent intermediate compositional terms. Therefore, for the scopes of this work the complete procedure of dust characterization (elemental and mineral composition, size distribution, optical properties and radiative downward flux) described in the following sections was applied only to the volcanics and travertine dust.

2.2 Individual particle microanalysis

An environmental scanning electron microscope Philips XL30 ESEM (FEI Company, tungsten filament) equipped with an energy dispersive spectrometer for x-ray microanalysis (EDAX/AMETEK Inc.,USA) was used for individual particle characterisation of the PM_{10} dust. Instrumental calibration of the magnification and of the XEDS spectrometer gain are routinely performed on the basis of the US EPA Guideline for SEM EDX microanalysis of particulate matter samples (Willis et al., 2002). A small portion of sample (about 8% of total filter area) was cut in the centre of polycarbonate membranes, fixed to aluminium stubs by self-adhesive carbon discs (TAAB, 12 mm diam.) and coated with an ultra-thin carbon layer by a vacuum evaporator (108 Carbon A, Cressington, Scientific Instruments Ltd., U.K.). SEM XEDS acquisitions were performed under high vacuum (10^{-6} hPa) at 20 keV accelerating voltage, allowing the K-line excitation of elements with atomic number Z Ò27 (Co, KŬ6.923 keV). Micrographs were acquired by secondary electron detector (SED) at magnification, working distance (WD), tilt angle and spot size conditions properly adjusted on a case-sensitive scale to optimize image resolution. The microanalysis was performed at WD 10 mm (take-off angle 35° relative to the specimen plane) on field areas of 1290 ï 5200 εm^2 (magnitude x 6000-3000) spread on the overall specimen surface; between 700 and 1000 particles were analysed per sample.

The Particle/phase analysis v.3.3 package (EDAX Inc., 2000) was used for the automated individual particle microanalysis; threshold of the digitalised object area to be analysed was set at 80%. Since a great number of individual particles was analysed, short live times (20ï 30 s) were imposed to XEDS spectra acquisition. Each field of microanalysis was manually selected prior to launching the automated scanning of particles. This choice allows a field-specific tuning of the grey scale, in order to minimize brightness *artifacts* in the automated identification of particles. Amplification time and spot size were adjusted to ensure dead time around 30% and total counts rate above 500 cps. In addition to automated microanalysis, manual acquisitions were carried out, both on field areas and on individual particles, by using the EDAX control v. 3.3 package (EDAX Inc., 2000). About 20 to 30 field areas were selected from the different dust samples to perform manual acquisitions. These have been run in triplicate on each field (live time 10 ï 20 s), to assess the repeatability of the microanalysis.

Further, XEDS spectra acquired from areas included in these fields were quantified by the conventional standard-based quantification procedure of bulk materials, to assess consistency with results previously obtained by ED-XRF analysis (Pietrodangelo et al., 2013).

Manual microanalysis of 15 to 30 individual particles per-sample was also performed, and high resolution micrographs of these particles were stored. Magnification above 6000x and longer live times (30 - 60 s) were employed, so that resulting XEDS spectra have total counts rate ranging 5000-10000 cps. These data were used both to assess the accuracy of microanalysis with respect to different mineral particles (Table 1), and to perform the quantification of individual-particle XEDS spectra by an internal standard approach, as further discussed in Sect. 2.3 and 3.1.1.

2.3 Quantification of individual particle XEDS spectra and procedure of particle allocation to mineral classes

A large data set of XEDS spectra and size (Feret diameters, area, aspect ratio, roundness) of individual dust particles was stored. To allocate dust particles into main mineral classes of our dust samples, an ad-hoc procedure has been adopted.

First, the bulk mineral composition of dust samples was determined by x-ray diffraction (XRD), to identify major minerals in the dust samples. Then, XEDS spectra of individual particles were semi-quantified and matched to spectra and to elemental composition of

reference pure minerals expected after XRD analysis. Results of matching were used to apportion individual particles into main mineral classes. Details are described below andin Appendix 1 of supplementary materials.

The mineralogical characterization of dust samples has been carried out on the 50 µm sieved dust fraction, by an automatic diffractometer Scintag X1, equipped with a Si(Li) detector using a Cu KŬtarget, under the following conditions: Ni-filtered radiation, step-scan modality (2° step = 0.02°), acquisition time of 10 s, operating at 45 kV and 40 mA. Quantification of minerals has been obtained according to procedures defined by Moore & Reynolds (1997).

A random orientation of particles was obtained by pressing 0.5 g of the 50 εm sieved materials with 5 atm for 10 s. Quantitative determinations were obtained by using appropriated standards and elaborating spectra as indicated in Giampaolo and Lo Mastro (2000). From XRD results and on the basis of previous geological analysis of the area, mineral species to which individual dust particles have to be apportioned were identified.
Allocation of individual dust particles analyzed by SEM XEDS to mineral classes can be carried out by matching XEDS spectra of particles to those of pure minerals.
However, XEDS spectra of some minerals can be not available; in this case, allocation can be performed by matching the quantified elemental composition of particles with that of pure minerals. Therefore, prior to this step, particle elemental composition has to be quantified.
When quantification of individual particle XEDS spectra is concerned, the use of conventional methods for bulk and thin polished materials (Castaing, 1951) imposes some critical limitations, and proper adjustments and assumptions for the theoretical treatment of X-ray generation and losses in the particulate matrix are needed (Armstrong and Buseck, 1975; Van Dyck et al., 1984; Choy l et al., 2005 and 2007).
In addition to bulk matrix effects, the particle size and shape play a major role in the mass, absorption and fluorescence effects of particulate matrices (Fletcher et al., 2011).

In this study, the mass effect (induced by particle thickness lower than the spot size of primary electron beam) was considered negligible. Dust particles selected for quantification, indeed, show an equivalent projected area diameter (assumed as particle thickness according to Kandler et al., (2007)) above 2µm, that is far larger than the spot size used (0.3 ÷ 0.4 µm average). However, energy losses due to particle absorption and fluorescence effects cannot be neglected. Among methods described in literature to quantify environmental particles by XEDS microanalysis (Fletcher et al., 2011), the particle standard approach was adopted in this

work. In particular, an internal standard was used; by this choice, particle matrix effects are included in the quantification process, and the conventional standard-based quantification method still can be used (Castaing's first approximation corrected for bulk matrix effects by the ZAF algorithm). Full details of this approach are described in Appendix I of supplementary materials.

Apportioned mineral particles of the volcanic and travertine dusts were then used to investigate the microphysical, optical and radiative properties of the PM10 lithogenic dust of Rome.

2.4 Size distribution

In this work, the assumption of particle sphericity has been adopted, due to the requirements of the 6SV code for radiative transfer modelling. Therefore, physical size of particles was assumed as the diameter of the equivalent spherical cross sectional area (ESD) (Reid et al., 2003; Kandler et al., 2007; Choël et al., 2007) measured by SEM. Then, mineral density was assigned to apportioned particles; volume, mass and aerodynamic diameter were consequently calculated (Kulkarni et al., 2011). On this basis, the volume size distributions of most representative mineral species observed in this study (kaolinite, quartz, feldspar and calcite) have been built.

2.4.1 Probability density function

The probability density functions (PDF) of the volcanics and travertine PM_{10} dust were estimated by fitting the frequency distribution of particle size to log-normal curve. Frequency distributions of volcanics and travertine were built on the basis of the 15 size bins of the GRIMM 1.108 optical particle counter (OPC). The fitting procedure was developed using the R-Project programming environment (R Core Team, 2013) and the routine was implemented by a nonlinear regression model based on a weighted-least-squares function (Ritz & Streibig, 2008).

The procedure attended to minimise the deviation between observed distribution and log-normal model. This is expressed by the equation (Davies, 1974):

$$\frac{dN(r)}{d\log r} = \frac{N}{\sqrt{2\pi}\log\sigma}\exp\left(\frac{-1}{2}\left(\frac{\log r - \log r_m}{\log\sigma}\right)^2\right)$$

where N is the number of particles, r_m is the mean radius of particles, and σ is the standard deviation of r. The uncertainty of each bin was estimated associating a Poisson error to the bin weight (Liley, 1992), that is calculating the square root of the total counts of particles observed in each size range. Quality assurance of the fitted models was evaluated considering the ñchi squaredò index (χ^2) in order to estimate the level of acceptance (Wilks, 2006).

This index is proportional to the sum of squares of the difference between each data point and the corresponding computed value. The level of acceptance was defined using the χ2 distribution tables.

2.5 Radiative transfer modelling

An atmospheric radiative transfer code was employed, to retrieve the optical and radiative dust properties. The 6SV (Second Simulation of a Satellite Signal in the Solar Spectrum ï Vector) (Vermote et al., 2006; Kotchenova et al., 2008) is the new-generation open-source atmospheric radiative transfer model 6S (Second Simulation of a Satellite Signal in the Solar Spectrum), (Vermote et al., 1997). This code is able to retrieve optical properties of the aerosol and to model the atmospheric radiative field by using the aerosol microphysical properties, under the hypothesis of spherical and dry particles. Microphysical properties of aerosol required for the modeling are the size distribution and refractive index. Size distributions targeted to the type of aerosol can be introduced as input in the 6SV code. To this aim, frequency distributions of particle size of the volcanics and travertine PM_{10} were processed for curve-fitting, as described in Sect. 2.4.1. Log-normal curve parameters r and σ of the two dust types were thus used as inputs in the 6SV code.

The real and imaginary parts of the refractive index (r.i.) were assumed from literature.
This choice was driven by the fact that the 6SV code requires as input the spectral trend of the real and imaginary parts of r.i., and these measurements were not available from our laboratory. Therefore, the refractive index of the ówater-insolubleôaerosol component reported in Kokhanovsky (2008) was associated to the volcanics dust of Rome area. This component is indeed defined as mainly dust, rich in water-insoluble minerals e.g. silicates, and is reported in literature in the spectral domain considered by the 6SV code. In the case of travertine dust, the calcite refractive index data reported by Ghosh (1999), Sokolik and Toon (1999) and Di Biagio et al. (2014) were used.

The 6SV code retrieves aerosol optical properties by the Mie Theory and simulates, afterword, the radiative modeling by solving the radiative transfer equation (RTE) in the solar spectral domain. By this way, the propagation of solar radiation in the Atmosphere/Earth coupled system can be completely described.

Runs of 6SV code were performed on a setting of parameters related to the site-specific meteorological and atmospheric conditions, and to the aerosol loading and microphysical properties. Concerning meteorological parameters, the profiles of temperature, pressure and humidity were assumed by the *1976 U.S. Standard* Atmosphere included in the 6SV code.

Atmospheric conditions were established in order to model the radiative field under daily *maximum Sun* elevation in Rome Area; a spring day, 12 May, at midday was thus selected. Columnar contents of water vapor and of ozone were fixed to 1.32 cm and 0.283 Db, respectively. To describe the aerosol loading, the aerosol optical thickness at 550 nm, τ_{550} (Vermote at al., 1997; Kaufmann et al., 1997; Bassani et al., 2010 and 2012) is commonly considered. The atmospheric profile of the aerosol is assumed to be exponential with a scale height of 2 km (Vermote at al., 1997). In this study, however, an higher value of aerosol optical thickness, $\tau_{550} = 0.7$, was chosen, in order to allow describing a scenario where the local geological dust loading has a major role when the radiative field in the atmosphere/earth coupled system is simulated.

Among optical properties, the single-scattering albedo and the asymmetry parameter were chosen, as they are crucial to perform analysis of the aerosol contribution on the radiative field (Dubovik et al., 2002; Kassianov et al., 2007).

Concerning the simulation of the radiative quantities, the downward irradiance was modelled, to the aim of performing a preliminary investigation on the radiative impact of the different dust types in the Earth-atmosphere coupled system. The volcanics and travertine PM_{10} local dust are expected to show significantly distinct microphysical properties, due to their compositional differences. Radiative modelling has been performed thus on the assumption of an atmosphere where the only aerosol component is volcanics or travertine dust, separately.

In order to evaluate the direct radiative effect at the surface of the two local dust components, the radiative forcing efficiency (RFE) at BOA has been considered. In a recent modelling study, Gomez-Amo et al. (2011) derives the RFE by using a radiative transfer code. In this study, the RFE has been computed for each component by the difference between the BOA

flux simulated by 6SV code in case of atmosphere with and without the dust component in the 250 - 4000 nm spectral domain and normalized with respect to the AOT at 550 nm (Garcia et al., 2008). The comparison between the RFE of volcanic and travertine allows to analyse the dependence of surface forcing from aerosol types (microphysical properties) and SSA independently from the aerosol loading (di Sarra, 2008, 2013; Di Biagio et al., 2010).

Results are showed in Sect. 3.5.2 and 3.5.3.

3 Results and discussion

Results of individual-particle XEDS spectra quantification and classification into mineral species are reported in Sect. 3.1 ï 3.3. In particular, the discussion concerns the reliability of microanalysis and of high-counts spectra quantification (Sect. 3.1), a principal component analysis (PCA) of particles elemental composition (Sect. 3.2), the allocation into mineral classes and the reliability of quantification by the internal standard approach used in this work (Sect. 3.3). In Sect. 3.4 volume size distributions are discussed, and differences between calcite from a lithogenic source (travertine dust) and from an anthropogenic material (paved road dust) are also evidenced. Finally, in Sect. 3.5 the microphysical and optical properties, and the downward component of radiative flux at BOA (Bottom Of Atmosphere) in a volcanics ï rich or travertine ï rich atmosphere are discussed, with respect to the features of Rome area.

3.1 Reliability of XEDS microanalysis and quantification

In Table 1 (upper part) the repeatability of XEDS microanalysis and consistency with the ED-XRF analysis are reported. Repeatability was evaluated by triple field acquisitions (number of fields: 20 ÷ 30) from each PM_{10} dust sample. Large fluctuations around mean (% relative standard deviation) are observed for light (Na and Mg principally) and trace (Mn and Ti) elements. Consistency with previously obtained elemental profiles of the PM_{10} fraction (Pietrodangelo et al., 2013) by ED-XRF, was assessed by matching to the latter the percent weight element composition of micro-areas of the dust samples obtained by XEDS field microanalysis. Results indicate that the microanalysis is less reliable for Na, Mn and for Si

and Mg in the siliciclastics sample, while in all other cases it shows a good agreement with ED-XRF bulk analysis.

Quantification results of manually acquired XEDS individual particle spectra are also reported in Table 1 (lower part), for kaersutite, quartz and calcite. Quartz and calcite represent the compositional end-members of mineral species observed in the dust samples of this work. Kaersutite particles were frequently observed during manual acquisitions. As this silicate mineral include in its composition non-negligible presence (above 4 %wt) of the principal crustal elements (Al, Na, Mg, K, Ca and Fe), it has been assumed as reference term for the microanalysis of silicate particles. XEDS spectra of kaersutite, calcite and quartz particles are showed in Fig. 3S, 4S and 5S, respectively.

The element composition is reported in terms of element mass in the electron interaction volume at 20 KeV; the latter was estimated for quartz, kaersutite and calcite according to Potts (1987). Uncertainties of quantification are large for K, Na, Mn and Ti, as expected due to the poor sensitivity of XEDS microanalysis to light and/or trace elements, whereas they range 1 ÷ 10 % relative error for other elements. Element uncertainties reported in Table 1 were estimated following the approach by Ziebold (1967), after assigning the proper peak-to-background ratio to each element in each mineral particle. The compositional differences of individual particles of quartz, calcite and kaersutite, with respect to related bulk mineral standards, are also reported in Table 1 (last rows) in terms of absolute percent differences between the element % wt in the standard mineral and that in the mineral particle.

As expected from the uncertainties, major compositional differences with respect to mineral standards are observed in Na, Mn and Ti quantification of kaersutite; also the quantification of Ca differs largely from the mineral standard, both in kaersutite and in calcite particles.

3.2 Elemental composition of individual dust particles

Particles included in the data set are individually codified with respect to the respective dust source, so that they are traceable in the statistical processing of data. Comparing information extracted from a multivariate statistical analysis of this data set, on the dust type to which each particle is ascribed, to same information certainly known from particle coding in the same data set, allows the evaluation of soundness of the elemental composition data and, consequently, of the quantification approach applied to particle XEDS spectra.

To this goal, a principal component analysis (PCA) of the elemental ratios commonly used to discriminate among different mineral classes (Al/Ca, Fe/Ca, K/Ca, Mg/Ca, Ti/Ca, Si/Al, Si/Fe, Ti/Fe and Ti/Mn) was performed. The XLSTAT 7.5 statistical package (Addinsoft) was used, with Varimax rotation and extraction of the latent factors; results are showed in Fig. 1 and 2. Three latent factors with eigenvalue higher than unity explain 76% of the total variance of particle composition. The element/Ca ratios mainly contribute to the first factor (F1, eigenvalue 4.5), the Si/Al and Si/Fe ratios contribute to the second factor (F2, eigenvalue 1.8), while the Ti ratios are represented by the third factor (F3, eigenvalue 1.3). In Fig. 1, particle scores are reported in the F2 vs F1 and in the F3 vs F2 plots.

Particles described by the F1 are ascribed to volcanics and, in minor fraction, to siliciclastics dust. The latter are indeed described mainly by the F2. Finally, road dust and travertine particles are grouped by the F3. Marlstone particles were not included in the PCA and in the subsequent parts of the study, due to the smaller number of available data with respect to the other samples. To assess the soundness of the PCA solution, the relative Si and Ca abundance and the equivalent spherical volume (ESV) have been examined, within clusters identified by the F1, F2 and F3. In Fig. 2, the Si and Ca abundances of particles with factor score higher than unity on each of the three latent factors have been plotted with respect to the ESV.

Since the average mass fractions of Si and Ca, in SiO_2 and $CaCO_3$ respectively, are 0.47 and 0.4, the threshold of 0.4 can be used to discriminate qualitatively either between silica and silicates (for which Si abundance is expected roughly below 0.4), and similarly between calcite and other Ca-bearing particles. Median Si abundance of both volcanics and siliciclastics particles in F1 is 0.37÷0.39 (Fig. 2a); also Ca abundance is similar in both particle groups (below 0.1). Median values of particle ESV are 3 μm^3 (volcanics) and 3.5 μm^3 (siliciclastic), although a very large variability was measured. Upon the above considerations on the Si mass fraction in SiO_2, a silicate nature of these particles might be supposed. Particles grouped by the F2 (Fig. 2b) are mainly siliciclastic and only a minor fraction is ascribed to volcanics. All these particles share both the Si and Ca abundances (0.6 and 0.1, respectively), and the median ESV (3÷3.5 μm3), the latter being comparable with the ESV of F1 particles. Si abundances far above 0.4 suggest that these are silica particles. It should be also noted that, as particles in F1 and F2 show similar ESV but different Si abundance, differences in the particle density can be supposed between these two groups. Finally,

particles with the highest score in F3 (Fig. 2c) are mainly ascribed to road dust and travertine samples and show Ca abundances around 0.4, which can be related to $CaCO_3$.

The PCA solution found on the XEDS data set of particle elemental composition is thus coherent with the real mineralogical nature (silicate or calcite) of particles, indicating that the sample-targeted internal standard approach applied to the quantification of particle composition provided reliable results.

3.3 Mineralogy of samples and allocation of individual particles

The mineralogical composition quantified by XRD analysis is reported in Table 2.

Main differences concern the increasing amount of calcite (volcanics < siliciclastic rocks < marlstones < travertine), the absence of inosilicates in siliciclastic rocks and travertine, the negligible amount of phyllosilicates in travertine and the considerable presence of quartz in siliciclastic rocks. All of these features are consistent with the geological processes involved in the formation of each rock type. Calcite is a geochemical marker of the sedimentary environment where rocks are formed and it is associated to the chemical precipitation of calcium carbonate. As a consequence of that, while its presence in volcanic rocks is negligible, in the marine deposits (marlstones) it is dominant and in the siliciclastic series it represents the second most abundant mineral component after phyllosilicates.

Moreover, it is the almost exclusive component of travertine, generated by the precipitation of CaCO3 near the hot hydrothermal springs of the Tivoli basin (Pentecost, 2005; Faccenna et al., 2010). The mineralogical composition of the silicate component in marlstones and siliciclastics dust is strictly related to the originating materials. Rock-forming processes (erosion, fluvial and marine transport, sedimentation) support, in this case, the presence in the PM_{10} fraction, as detected by XRD, of stable silicates (plagioclase and quartz), the reduced presence of inosilicates and the presence of alteration by-products, such as phyllosilicates. Different processes must be considered in volcanic rocks, which explain the mineralogical composition of silicates observed in the PM_{10} resuspended from this geological material; specifically, crystallization is the main responsible process, in this case. Thus, the presence of most minerals observed in the PM_{10} from volcanic rocks is coherent with the magmatological framework of Central Italy. Differently from the above considerations, however, the association kaolinite ï quartz, observed by SEM XEDS microanalysis in this PM_{10} dust type,

has to be ascribed to rock alteration (weathering). In this case quartz is thus the product (with kaolinite) of the hydrolysis reaction of feldspars (Jackson et al., 2010), and not a crystallization-derived phase.

Considering the results of the allocation procedure (Sect. 2.3), mineral particles in the PM_{10} dust samples were mainly classified as: phyllosilicates (kaolinite, smectite and micas), representing more than half of the silicate (non-quartz) fraction of the totality of samples, tectosilicates (feldspar, chabazite, leucite and plagioclase) and inosilicates (clinopyroxene and amphibole), which contribute comparably to the rest of silicate fraction, quartz and calcite. About 65% (percent abundance) of total phyllosilicates are found in the volcanics, being mainly kaolinite (observed in the volcanics only) and 60% of total observed smectite. Micas are also frequently observed, mainly in the siliciclastics sample. Concerning tectosilicates, the overall contribution apportioned to the PM_{10} of each geological domain and of road dust has been found to be 47% in the volcanics, 20% in the siliciclastic rocks, 33% in the road dust, while it appears negligible in the marlstones. Inosilicates were observed in similar amounts, and solely in the volcanics and in the road dust. About half of quartz particles identified in the totality of PM_{10} dust samples is apportioned to siliciclastic rocks, while volcanics, marlstone and road dust provide equally to the remaining fraction. Finally, within the non-travertine sedimentary rocks of this study, the marlstones provide the most important contribution of calcite particles in the PM_{10} fraction (ab. 35%), while the contribution of siliciclastic rocks is around 8%. Similar contributions than marlstones are also apportioned to road dust. These results, obtained by the allocation procedure, are in good agreement with the mineralogical composition by XRD (Table 2).

To assess the reliability of allocation, a mass closure approach was used.

The particulate mass fraction of each mineral group in the PM_{10} (sum of particles mass within a mineral group, per dust sample) was estimated from results of the allocation after SEM XEDS microanalysis. Afterwards, the PM_{10} weight percent composition of the total silicate (including quartz) content and of the calcite content were calculated; these quantities were then compared to the corresponding quantity obtained by XRD analysis of the 50μm sieved fraction of each dust sample, as reported in Fig. 3.

Although the travertine was not analyzed by XRD, since it can be considered a pure calcite term (Pentecost, 2005), results of the SEM XEDS microanalysis of the travertine dust have been reported for this sample too. In all dust samples (excluding the case of travertine), a good comparability with analytical results of mineral composition by XRD are observed for

mass estimates obtained from the allocation of individual particles. Besides indicating that the allocation procedure produced reliable results, this also suggests that the silicate and calcite contents of the PM_{10} and of the 50μm sieved fractions of dust are likely similar, as yet reported in literature (Rashki et al., 2013).

3.4 Connections between geochemical processes of rock sources and the PM_{10} fraction of minerals

The size distribution of re-suspended geological materials is influenced by two important contributions: the physical properties of particles (e.g. size and density), which affect the dust resuspension and transport; and the geological features of the rock source, which determine the particle mineralogical identity. In this view, size distribution of the PM10 fraction has been discussed either for individual mineral species (quartz, kaolinite, feldspars and calcite), or for the overall local lithogenic dusts (volcanics, siliciclastic rocks and travertine); in the latter case the totality of mineral particles identified in each dust type was considered. In Sect. 3.4.1, size distributions of individual mineral species have been investigated with respect to the clay fraction according to Claquin et al. (1999), Nickovic et al. (2012), and Journet et al. (2014), while in Sect. 3.4.2 volume distributions (Formenti et al., 2014) of mineral species and of lithogenic dusts are discussed.

3.4.1 Clay fraction of minerals

In this part of the study the classified mineral particles were treated with respect to the geochemical processes which they can be related to, with the aim of relating the size distribution of each mineral species to the geochemical processes acting on the rocks to generate the PM_{10} fraction of that mineral species. Therefore particles are here named as: - phyllosilicates, including clay-minerals (kaolinite, illite, smectite and chlorite groups), and representing thus the contribution of weathering and pedogenesis to the resuspension from outcropping rocks; - ǿother silicatesô, including phases such as plagioclase, K-feldspar, pyroxene and quartz, which can be considered as crystallization products in volcanics rocks, or debris phases in sedimentary rocks; -calcite, differentiated by lithogenic and road dust particles. The approach of Claquin et al. (1999) was adopted in choosing mineral species for

which the mass percentage in the clay fraction (particle size < 2 µm) was calculated, on the basis of the particle ESD. Mass percentages of mineral in the clay fraction of PM_{10} dust samples of this study were compared with those obtained by Journet et al. (2014) for the modelled global yearly average composition of airborne minerals. With respect to the latter (abbr. *gyac*), the mineral composition of the Rome local geological PM_{10} shows the following similarities, or discrepancies: 1. the amount of quartz in the clay fraction of the siliciclastic PM_{10} (20%) and of the volcanics PM_{10} (8%) is significantly higher compared to the *gyac* (4.9%); 2. feldspars in the clay fraction of both the volcanics (4%) and siliciclastic PM_{10} (2.5%) are comparable to feldspars in the *gyac* (3.6%); 3. kaolinite dominates the clay fraction of the volcanics PM_{10} (63%) and it is negligible in the other PM_{10} dust types (ca. 2.5%), while in the *gyac* it represents 24.1% of total mass; 4. smectite in the Rome local geological PM_{10} ranges 3 to 10%, that is lower compared to *gyac* (15.3%).

With respect to the mineralogical profiles of PM_{10} dust from sources located in North Africa (N.A.) and Saudi Arabia (S.A.) (Ganor et al., 2009), the dust samples of this study show the following differences: 1) large variability in terms of calcite content (up to 90% in travertine), compared to PM_{10} from N.A. and S.A. (20-30%); 2) large variability in terms of tectosilicates (up to 20% in volcanics) and clay minerals (up to 57% in volcanics) compared to PM_{10} from N.A. and S.A. (1-3% 30-40% respectively); amount of quartz comparable to that in PM_{10} from N.A. and S.A. (2-4%) in the case oft he siliciclastic PM_{10}, but significatively different in travertine (undetectable) and in volcanics (10%). Moreover, the presence of inosilicates is not reported for the PM_{10} from N.A. and S.A., while the latter show the presence of gypsum, not observed in the PM_{10} dust samples of this study.

Considering the distribution of particles in the clay and non-clay (ESD > 2 µm) fractions of the mineral PM_{10} of Rome area, main differences are observed between the volcanics and the travertine types. In the volcanics PM_{10} the weathering by-products (quartz, kaolinite and smectite) are comparably distributed in the two size fractions, indicating that weathering processes produce either small grain-sized crystals, and altered phases which grow on the surface of large crystals, resulting in larger particles. The crystallization phases produced in the volcanics PM_{10} (feldspars and pyroxene) are instead enriched in the non-clay size, as implied in the crystallization process.

Source-related differences between natural calcite from travertine and calcite from road dust were also evidenced. The clay/non-clay distributions of calcite in the PM_{10} of either the

travertine dust and the road dust travertine-related, differ significantly from the clay/non-clay calcite distribution in the PM_{10} of road dust volcanics-related. While in the first case the calcite is comparably distributed in the clay/non-clay size, the mass percentage of this mineral in the road dust volcanics-related is higher in the clay size (80%) than in the coarser size (60%). Since the presence of calcite in the volcanics PM_{10} is negligible, calcite content in the PM_{10} road dust collected in the volcanics can only be ascribed to the asphalt contribution.

It is thus reasonable that this anthropogenic source enrichs the size fraction below 2 µm (ESD) of calcite, more than the coarser one. This effect is less evident, instead, in the road dust travertine-related, where the lithological influence of travertine rocks assumes a major role in the clay/non-clay distribution of calcite.

3.4.2 Volume size distribution of the PM_{10} fraction: minerals and lithogenic dust types

The volume size distributions of quartz, feldspars, kaolinite and calcite are reported in Fig. 4 versus the aerodynamic diameter (a.d.); in this figure, particles have been grouped with respect to belonging to a given mineral species, without differentiating by geological domain. Fig. 4a shows the distributions of kaolinite, quartz and feldspars, while in Fig. 4b distributions of calcite in the two different road dust types and in travertine are shown.

Volume distributions of the considered silicates are unimodal, with overlapping maxima around 5 µm. Main differences are in the peak width: weathering minerals, such as kaolinite, show a broader curve, compared to minerals from crystallization phases, e.g. feldspars. This is coherent with the above described action of the weathering, of generating particles either in the clay-fraction, and in the coarser size, which contributes to broaden the size range.

Quartz shows an intermediate behaviour, due to different processes acting on quartz formation: weathering in the volcanics, crystallization in the siliciclastics.

The different nature of geochemical processes affects also volume distributions of the overall lithogenic dust types (Fig. 4c). Particularly, volcanics and siliciclastics dusts show broader distribution than travertine, due to the dominance of weathering, in the formation of lithogenic PM_{10} from volcanic and siliciclastic rocks, with respect to the importance of crystallization in the travertine domain.

More defined differences are highlighted among the volume distributions of calcite from lithogenic or anthropic source: in PM_{10} from travertine, the volume distribution of calcite shows a very narrowed shape, with maximum at 5 µm. Conversely, calcite of both road dust types shows broader distributions, extended to finer sizes, especially in the case of the volcanics-related road dust. In the latter, the curve is bimodal with maxima at 3.8 µm and 1.8 µm, while in the travertine-related it is unimodal, with maximum at 5.3µm similarly to calcite in travertine. The lithogenic or anthropic nature of processes tuning calcite size also influence the height of volume distributions of calcite.

In the first case, calcite particles mainly originate from crystals formed in the precipitation of calcium carbonate, as explained in Sect. 3.3; the variability of particle size is thus limited by chemical ï physical conditions which rule travertine formation. In the second case, the variety of mechanical solicitations affecting the surface of paved roads, e.g. abrasion by vehicle riding, is described by a wider particle size range.

Discrepancies observed within volume distribution curves of Fig. 4 suggest also that individual particle densities may differ within the same silicate species or within calcite from different dust sources. It is acknowledged that the density of mineral particles may range significantly due to the petrological conditions (chemistry, kinetics and thermodynamics involved in the crystallization process) associated to the different crystallization phases, by which mineral particles are formed.

In addition, some general considerations can be given on the particle density, by taking into account the distribution of particle mass percentage (discussed in Sect. 3.4.1) and ESD, with respect to the below/above 2 µm size threshold (coherently with the clay / non-clay distribution). Decreasing particle density should be expected from first to last of the following cases: 1. both mass percentage and ESD of particles mainly distributed below 2 µm; 2. mass percentage mainly observed below the 2 µm size and ESD comparably distributed with respect to this threshold; 3. both mass percentage and ESD mainly distributed in the size fraction above 2 µm. In Fig. 4, first case can be related to the calcite of road dust volcanics-related (80% of particles showing ESD < 2 µm), while second case applies to quartz and kaolinite, and last case to feldspars and travertine calcite (60% and 80%, respectively, of particles showing ESD > 2 µm).

Height differences among volume distributions of the dust types can be thus explained in connection with the different presence of a given mineral species in a dust type. In particular,

while the content of kaolinite is higher in the volcanics than in siliciclastic dust, feldspars and quartz are more abundant in the latter. It is thus possible that these minerals play contrasting roles in defining the average particle density of siliciclastic dust, and consequently its volume distribution.

3.5 Microphysical, optical and radiative properties of the volcanics and travertine PM_{10} dust in the Rome area

3.5.1 Microphysical properties

In Fig. 5 results of the fitting procedure to log-normal curve, applied to volcanics and travertine size distribution, are shown.

The curves are reported with respect to the particle physical radius, as required by the 6SV radiative transfer code. The computed ñchi squaredò (χ^2) of fitting are respectively 0.34 for volcanics and 0.69 for travertine. Considering twelve degrees of freedom corresponding to the 13 size bins of the optical particle counter, both fitting are below the level of significance of 99.5%. It is thus possible to refuse the null hypothesis that these curves cannot be fitted to a log-normal function. The following r_m and σ values of the volcanics and travertine size distributions are used thus, as input parameters of the Log-normal function (Eq. 1):

$r_m^{volc} = 1.64 \pm 0.29$ μm, $\sigma^{volc} = 1.85 \pm 0.23$ μm;

$r_m^{trav} = 1.39 \pm 0.72$ μm, $\sigma^{trav} = 2.34 \pm 0.46$ μm.

Results of fitting are in line with findings discussed by Mahowald et al. (2014).

The other microphysical property required for 6SV run is the refractive index. In Fig. 6 the real (n) and imaginary (k) part of the refractive index have been interpolated at the 6SV twenty wavelengths (350; 400; 412; 443; 470; 488; 515; 550; 590; 633; 670; 694; 760; 860; 1240; 1536; 1650; 1950; 2250; 3750 nm), following the spectral data of water-insoluble (Kokhanovsky, 2008; WCP-112, 1986) and calcite-rich dust (Ghosh, 1999) refractive index, respectively related to volcanics and travertine. While the spectral trend of volcanics refractive index follows the commonly adopted trend used in the radiative transfer modelling (RTM) of the dust component (Kokhanovsky, 2008), the travertine dust, being mainly composed of calcite, is a non-absorbing aerosol in the spectral range considered in this study,

as in this range the imaginary part of calcite refractive index is close to zero (Sokolik and Toon, 1999; Ghosh, 1999; Di Biagio et al., 2014 ,).

3.5.2 Optical properties

Optical properties of the volcanics and travertine contribution to Rome local mineral dust have been modeled in the twenty wavelengths of the 6SV code. In Fig. 7 the single-scattering albedo (SSA) and the asymmetry parameter (g) are shown, which are critical to analyze the aerosol-induced at-ground radiative flux (Kassianov et al., 2007). The lower SSA of volcanics, with respect to travertine, attests that the volcanics dust absorbs the solar radiation in the VISible (VIS) spectral domain, as commonly expected for mineral dust. Conversely, the SSA of travertine indicates that this dust type is a non-absorbing particulate. In Fig. 7b the spectral dependence of the asymmetry parameter (g) is showed for the volcanics and the travertine. As g is higher in the volcanics, in this dust type particles show higher forward scattering than in the travertine, mainly in the Near-InfraRed (NIR) spectral domain. These findings suggest that the local geological dust of the Rome area affects both the VIS and NIR spectral domains; consequently an influence on the radiative field is expected as well.

3.5.3 Downward radiative flux at Bottom Of Atmosphere (BOA)

The radiative modeling has been focused on the downward component of the radiative impact at BOA due to the volcanics and travertine dust in Rome area. This part of the study represents a preliminary investigation of the direct radiative effect of the local dust component on the solar radiation at ground. In Fig. 8a the influence of both local dust types to the downward BOA solar irradiance (I) in the VIS and NIR spectral domain is shown. In order to evaluate the spectral dependence of the irradiance on the mineralogical composition of dust, the volcanics/travertine ratio is reported in Fig. 8b. In the VIS domain, the irradiance seems not to be affected by the mineralogical composition, as the BOA downward irradiance trends of two dust types almost overlap. However, in the NIR a sharp discrimination between the radiative impact of the volcanics and that of the travertine dust is revealed. Finally, the BOA downward flux obtained by integrating the downward solar irradiance over the solar spectral domain (250 - 4000 nm) is reported in Fig. 9. Both volcanic and travertine dusts leave the direct component unchanged, while the diffuse component depends strongly on the mineral composition. The scattered radiation of an atmosphere rich in travertine dust shows an higher

diffuse component than in the case when a volcanics ï rich atmosphere is considered. As a matter of fact, in the Rome site the total BOA downward flux is greater for an atmosphere where the only dust component is the travertine dust with respect to the sole presence of volcanic dust.

The evaluation of the radiative budget at surface of the local mineral dust in Rome area has been performed computing the RFE. The RFE is calculated by simulating the total BOA downward flux with the local dust component in three conditions of AOT at 550 nm (0.2; 0.5; 0.7), to estimate the uncertainty on the simulated RFE. The results highlight the stronger cooling effect at the surface in case of volcanic (-293 ± 17 W/m2) respect to travertine (-139 ± 7 W/m2) with uncertainties lower than 5%.

The aerosol radiative behaviour follow the general trend explained in Gomez-Amo et al., (2011), that is aerosols with high SSA (low absorption, travertine in case) produce a decrease in the absolute value of RFE, with respect to aerosols t characterized by high absorption, like the volcanics.

These results need to be confirmed by a more in-depth analysis on the influence of the local geological dust re-suspended from topsoil on the Earth ï atmosphere radiative balance, in Rome area.

4 Conclusions

In this work, a knowledge gap was faced, which concerns how, and to which extent, the mineral dust locally re-suspended from rocks outcropped in a site/area may influence the composition of airborne aerosol, the direct interaction (light scattering and absorption) of the aerosol with solar radiation, and the radiative flux at BOA (Bottom Of Atmosphere), within the same source area of dust. To this goal, a methodology was developed, which is suitable for general application; nevertheless, results reported here are intrinsically narrowed to the features of Rome area. Investigation was carried following three paths: site-specific analysis of the geochemical and mineralogical environment, individual-particle based instrumental analysis aimed at determining the mineralogical and microphysical properties of dust, and modelling of the dust radiative effects with respect to optical features.

Main results concern relationships found between: 1.geochemical processes acting on the source rocks and mineral species associated to particles in the re-suspended PM_{10} fraction of

different local dust types; 2. mineral composition of the PM_{10} dust and variability of dust microphysical properties (refractive index and size distribution); 3. dust-specific optical properties (single-scattering albedo and asymmetry parameter) of the PM_{10} fraction, and total downward flux at BOA in the VISible and Near Infrared (NIR) spectral domains.

First issue was discussed on all major outcropped domains in the Rome area (volcanic rocks, siliciclastic rocks, limestones, marlstones and travertine), and on the distinction between calcite from lithogenic source and calcite from paved road dust, while second and third issues focused on the compositional end-member of local dust types (volcanics and travertine).

With the exception of pure calcite (associated to PM_{10} from the travertine domain (Tivoli basin), and from road dust), PM_{10} dust types of the studied area show silicate-prevalent or calcite-prevalent compositions, depending on the outcropped source rocks: volcanics or siliciclastics in the first case, marlstones or limestones in the second case.

Rock weathering processes tune the size and mineral identity of PM_{10} particles in the silicate-prevalent dust types, more than other processes (e.g. debris formation, crystallization). On the other side, chemical precipitation of $CaCO_3$ influences mainly the particle composition of calcite-prevalent dust types. These differences reflect in the volume distributions, either of individual mineral species (kaolinite, quartz, feldspars, calcite), or of dust types.

Weathering processes can be related to larger size variability observed for some mineral species (e.g. kaolinite and quartz), with respect to feldspars and to lithogenic calcite.

In the lithogenic PM_{10} of Rome area, these minerals are instead mainly associated to crystallization or to $CaCO_3$ precipitation, occurring under defined chemical, kinetic and thermodynamic conditions which limit particle size and result in narrow volume distribution.

Differences observed between calcite from lithogenic source and calcite from road dust suggest a major role of the variability of mechanical solicitations from vehicular riding on the particle size of road dust calcite. Volume distribution of the latter interestingly shows bimodal shape, broader width and larger contribution to fine fraction, differing significantly from lithogenic calcite and from other investigated mineral species.

These findings indicate that the microphysical properties of different crustal components (e.g. road dust, dust from building activities, transported mineral dust, etc.) may differ consistently with source type; optical properties are reasonably expected to differ consequently.

Spectral trends of the complex refractive index related to volcanics and travertine PM_{10}, in the VIS and NIR domains, show that travertine PM_{10} is a non-absorbing dust, opposite to volcanics PM_{10}. We showed that these differences influence the diffuse component of BOA

downward flux, which is higher in the simulated case of a travertine-rich atmosphere, coherently with the non-absorbing behavior of this dust type.

Finally, it is important to underline that above results could be assessed only by considering the entire solar spectral domain, instead of limiting the investigation to the VIS region.

The radiative effects of the two components in the 350 - 3750 nm spectral domain have been evaluated by the RFE; results show higher efficiency of volcanic (-293 ± 17 W/m2) in surface cooling effect, with respect to travertine (-139 ± 7 W/m2), as expected for aerosol with SSA smaller than 1 (Di Biagio et al., 2010), that is the volcanics dust in this case.

Further research on these issues is needed, thus, as it may aid improving knowledge on the local effects of the presence of different crustal (natural or anthropic) components of aerosol at a specific site/area, in terms of aerosol interaction with solar radiation and radiative effects at BOA.

Acknowledgements

Thanks are due to Sergio Lo Mastro (Roma Tre University, Department of Geology, Rome, Italy), for X-ray diffraction analysis of the dust samples of this study. The authors are also grateful to Andrea Valdrè (FEI Company, U.S.), for his valuable scientific and technical advice with SEM XEDS microanalysis. Finally, we are grateful to Alcide di Sarra (ENEA, Laboratory for Earth Observations and Analyses) for helpful comments and suggestions that greatly improved the radiative transfer issues in the manuscript.

References

Aimar, S., Mendez, J. M., Funk, M., Buschiazzo, D. E.: Soil properties related to potential particulate matter emissions (PM10) of sandy soils, Aeolian Res., 3, 437-443, 2012.

Armstrong, J. T. and Buseck, P. R.: Quantitative chemical analysis of individual microparticles using the electron microprobe: theoretical , Anal. Chem., 47, 13, 2178-2192, 1975.

Bassani, C., Cavalli, R., Antonelli, P.: Influence of aerosol and surface reflectance variability on hyperspectral observed radiance, Atmos. Meas. Tech., 5, 1139ï 1203, doi:10.5194/amt-5-1193-2012, 2012.

Bassani, C., Cavalli, R.M., Pignatti, S.: Aerosol optical retrieval and surface reflectance from airborne remote sensing data over land, Sensors, 10, 6421ï 6438, doi:10.3390/s100706421,

2010.

Bergstrom, R. W., Russell, P. B., and Hignett, P.: Wavelength Dependence of the Absorption of Black Carbon Particles: Predictions and Results from the TARFOX Experiment and Implications for the Aerosol Single Scattering Albedo, J. Atmos. Sci., 59, 567-577, 2002.

Bevington, P. R. and Robinson, D. K.: Data Reduction and Error Analysis for the Physical Sciences, 2d Ed., McGraw-Hill, New York, 1992.

Buseck, P. R. and Pósfai, M.: Airborne minerals and related aerosol particles: Effects on climate and the environment, Proc. Natl. Acad. Sci. USA, 96, 3372ï 3379, Colloquium Paper, 1999.

Caquineau, S., Gaudichet, A., Gomes, L., Legrand M.: Mineralogy of Saharan dust transported over northwestern tropical Atlantic Ocean in relation to source regions, J. Geophys. Res., 107, D15, 4251, doi: 10.1029/2000jd000247, 2002.

Castaing, R.: Application des sondes électroniques à une méthode d'analyse ponctuelle chimique et cristallographique: publication ONERA (Office national d'études et de recherches aéronautiques/ Institute for Aeronautical Research) N. 55 (PhD Thesis), University of Paris, Paris,1952.

Choobari, O. A., Zawar-Reza, P., Sturman, A.: The global distribution of mineral dust and its impacts on the climate system: A review, Atmos. Res., 138, 152ï 165, 2014.

Choy l, M., Deboudt, K., Flament, P.: Evaluation of quantitative procedures for x-ray microanalysis of environmental particles, Microsc. Res. Techniq., 70, 11, 996-1002, doi: 10.1002/jemt.20510, 2007.

Choy l, M., Deboudt, K., Osán, J., Flament, P., Van Grieken, R.: Quantitative Determination of Low-Z Elements in Single Atmospheric Particles on Boron Substrates by Automated Scanning Electron Microscopy-Energy-Dispersive X-ray Spectrometry, Anal. Chem., 77, 5686-5692, 2005.

Claquin, T., Schulz, M., Balkanski, Y. J.: Modeling the mineralogy of atmospheric dust sources, J. Geophys. Res., 104, D18, 22,243-22,256, 1999.

Cosentino, D., Cipollari, P., Di Bella, L., Esposito, A., Faranda, F., Giordano, G., Gliozzi, E., Mattei, M., Mazzini, I., Porreca, M., Funiciello, R.: Tectonics, sea level changes and palaeoenvironments in the early Pleistocene of Rome (Italy), Quaternary Res., 72, 143-155, 2009.

Costantini, E. A. C., Urbano, F., Aramini, G., Barbetti, R., Bellino, F., Bocci, M., Bonati, G., Fais, A., LôAbate, G., Loj, G., Magini, S., Napoli, R., Nino, P., Paolanti, M., Perciabosco M., and Tascone, F.: Rationale and methods for compiling an Atlas of desertification in Italy, Land Degrad. Develop., 20, 261ï 276, doi: 10.1002/ldr.908, 2009.

DôAlmeida, G. A., Koepke, P., and Shettle, E. P.: Atmospheric Aerosols, Global Climatology and Radiative Characteristics. A. Deepak Publishing, Hampton, VA, 1991.

DôAlmeida, G. A.: On the variability of desert aerosol radiative characteristics, J. Geophys. Res., 92, D3, 3017-3026, 1987.

Davies, C. N.: Size distribution of atmospheric particles, Aerosol Sci., 5, 293-300,1974.

Di Biagio, C., di Sarra, A., Meloni, D., Monteleone, F., Piacentino, S., Sferlazzo, D.: Measurements of Mediterranean aerosol radiative forcing and influence of the single scattering albedo, J. Geophys. Res., 114, D06211, doi:10.1029/2008JD011037, 2009.

Di Biagio, C., di Sarra, A., Meloni, D.: Large atmospheric shortwave radiative forcing by Mediterranean aerosol derived from simultaneous ground-based and spaceborne observations, and dependence on the aerosol type and single scattering albedo, J. Geophys. Res., 115, D10209, doi:10.1029/2009JD012697, 2010.

Di Biagio, C., Boucher, H., Caquineau, S., Chevaillier, S., Cuesta, J., and Formenti, P.: Variability of the infrared complex refractive index of African mineral dust: experimental estimation and implications for radiative transfer and satellite remote sensing, Atmos. Chem. Phys., 14, 11093ï 11116, doi: 10.5194/acp-14-11093-2014, 2014.

di Sarra, A., Pace, G., Meloni, D., De Silvestri, L., Piacentino, S., Monteleone, F.:Surface shortwave radiative forcing of different aerosol types in the central Mediterranean, Geophys. Res. Lett., 35, L02714, doi:10.1029/2007GL032395, 2008.

di Sarra, A., Fuà, D., Meloni, D.: Estimate of surface direct radiative forcing of desert dust from atmospheric modulation of the aerosol optical depth, Atmos. Chem. Phys., 13, 5647-5654, doi:10.5194/acp-13-5647-2013, 2013.

Dobrzhinsky, N., Krugly, E., Kliucininkas, L., Prasauskas, T., Kireitseu, M., Zerrath, A., Martuzevicius, D.: Characterization of desert road dust aerosol from provinces of Afghanistan and Iraq, Aerosol Air. Qual. Res., 12, 1209-1216, 2012.

Downs R. T: The RRUFF Project: an integrated study of the chemistry, crystallography, Raman and infrared spectroscopy of minerals, 19th General Meeting of the International Mineralogical Association in Kobe, Japan, July 23-28, O03-13, 2006.

Dubovik, O. and King, M. D.: A flexible inversion algorithm for retrieval of aerosol optical properties from Sun and sky radiance measurements, J. Geophys. Res.,105, D16, 20,673-20,696, 2000.

Dubovik, O., Holben, B., Eck, T. F., Smirnov, A., Kaufman, Y. J., King, M. D., Tanré, D., and Slutsker, I.: Variability of absorption and optical properties of key aerosol types observed in worldwide locations, J. Atmos. Sci., 59, 590-608, 2002.

Dürr, H. H., Meybeck, M., Dürr, S. H.: Lithologic composition of the Earthôs continental surfaces derived from a new digital map emphasizing riverine material transfer, Global Biogeochem. Cy., 19, GB4S10, doi:10.1029/2005GB002515, 2005.

Evans, R. D., Jefferson, I. F., Kumar, R., Hara-Dhand, K. O., Smalley, I. J.: The nature and early history of airborne dust from North Africa in particular the Lake Chad basin, J. Afr. Earth Sci., 39, 81ï 87, 2004.

Faccenna, C., Funiciello, R., Soligo, M.: Origin and deposition of the Lapis Tiburtinus travertine, in: The Colli Albani Volcano: Funiciello, R. and Giordano, G. Editors, Geological Society of London, 215, ISBN: 978-1-86239-307-3, 2010.

Falkovich, A. H., Ganor, E., Levin, Z., Formenti, P., Rudich, Y.: Chemical and mineralogical analysis of individual mineral dust particles, J. Geophys. Res., 106, D16, 18,029-18,036, 2001.

Feng, G., Sharratt, B., Wendling, L.: Fune particle emission potential from loam soils in a semiarid region, Soil Sci. Soc. Am. J., 75, 2262ï 2270, 2011.

Fletcher, R. A., Ritchie, N. W. M., Anderson, I. M., Small, J. A.: Microscopy and microanalysis of individual collected particles, in: Aerosol Measurement: Principles, Techniques, and Applications, 3rd Ed.: Kulkarni, P., Baron, P.A. and Willeke, K. Editors, John Wiley & Sons Ltd, U.S., chapter 10, 195-198, 2011.

Formenti, P., Caquineau, S., Desboeufs, K., Klaver, A., Chevaillier, S., Journet, E., and Rajot, J. L.: Mapping the physico-chemical properties of mineral dust in western Africa: mineralogical composition, Atmos. Chem. Phys., 14, 10663ï 10686, doi:10.5194/acp-14-10663-2014, 2014.

Ganor, E., Stupp, A., and Alpert, P.: A method to determine the effect of mineral dust aerosols on air quality, Atmos. Environ., 43, 5463ï 5468, 2009.

Garcìa, O. E., Dìaz, A. M., Expòsito, F. J., Dìaz, J. P., Dubovik, O., Dubuisson, P., Roger, J.-C., Eck, T. F., Sinyuk, A., Derimian, Y., Dutton, E. G., Schafer, J. S., Holben, B. N., Garcìa, C. A.: Validation of AERONET estimates of atmospheric solar fluxes and aerosol radiative

forcing by ground-based broadband measurements, J. Geophys. Res., 113, D21207, doi:10.1029/2008JD010211, 2008.

Geoportale Nazionale, http://www.pcn.minambiente.it/GN/ MATTMï Ministero dellôAmbiente e della Tutela del Territorio e del Mare, Italy, 2011.

Ghosh, G.: Dispersion-equation coefficients for the refractive index and birefringence of calcite and quartz crystals, Opt. Commun., 163, 1ï3, 95-102, doi:10.1016/S0030-4018(99)00091-7, 1999.

Giampaolo, C. and Lo Mastro, S.: Analisi (semi) quantitativa delle argille mediante diffrazione a raggi X, In Fiore, S. (Editor.), Incontri Scientifici, Istituto di ricerca sulle argille, Vol. II, p 109-146 2000.

Gill, T. E., Zobeck, T. M., Stout, J. E.: Technologies for laboratory generation of dust from geological materials, J. Haz. Mat., 132, 1-13, 2006.

Goldstein, J. I., Williams, D. B., Cliff, G.: Quantitative x-ray analysis, in: Principles of Analytical Electron Microscopy: Joy, D. C., Romig Jr., A. D., and Goldstein, J. I. Editors, chapter 5, Springer U.S., ISBN: 978-1-4899-2039-3, 1986.

Gómez-Amo, J.L., Pinti, V., Di Iorio, T., di Sarra, A., Meloni, D., Becagli, S., Bellantone, V., Cacciani, M., Fuà, D., Perrone, M.R.: The June 2007 Saharan dust event in the central Mediterranean: Observations and radiative effects in marine, urban, and sub-urban environments, Atmospheric Environment, Volume 45, Issue 30,Pages 5385-5393, ISSN 1352-2310, doi:10.1016/j.atmosenv.2011.06.045, 2011.

Hansell Jr., R. A., Reid, J. S., Tsay, S. C., Roush T. L., and Kalashnikova, O. V.: A sensitivity study on the effects of particle chemistry, asphericity and size on the mass extinction efficiency of mineral dust in the earthôs atmosphere: from the near to thermal IR, Atmos. Chem. Phys., 11, 1527ï1547, 2011.

Jackson, M., Deocampo, D., Marra F., and Scheetz, B.: Mid-Pleistocene Pozzolanic volcanic ash in ancient Roman concretes, Geoarchaeology, 25, 1, 36-74, 2010.

Jeong, G. Y.: Bulk and single-particle mineralogy of Asian dust and a comparison with its source soils, J. Geophys. Res., 113, D02208, 4251-, doi: 10.1029/2007jd008606, 2008.

Journet, E., Balkanski, Y., and Harrison, S. P.: A new data set of soil mineralogy for dust-cycle modeling, Atmos. Chem. Phys., 14, 3801-3816, 2014.

Kalashnikova, O. V. and Sokolik, I. N.: Importance of shapes and compositions of wind-blown dust particles for remote sensing at solar wavelengths, Geophys. Res. Letters, 29, 10, 1398-, doi: 10.1029/2002GL014947, 2002.

Kalashnikova, O. V. and Sokolik, I. N.: Modeling the radiative properties of non-spherical soil-derived mineral aerosols, J. Quant. Spectrosc. Radiat. Transfer, 87, 137ï 166, 2004.

Kandler, K., Benker, N., Bundke, U., Cuevas, E., Ebert, M., Knippertz, P., Rodríguez, S., Schütz, L., Weinbruch, S: Chemical composition and complex refractive index of Saharan Mineral Dust at IzaÑa, Tenerife (Spain) derived by electron microscopy, Atmos. Environ., 41, 8058ï 8074, 2007.

Kandler, K., Schütz, L., Deutscher, C., Ebert, M., Hofmann, H., Jäckel, S., Jaenicke, R., Knippertz, P., Lieke, K., Massling, A., Petzold, A., Schladitz, A., Weinzierl, B., Wiedensohler, A., Zorn, S., Weinbruch, S.: Size distribution, mass concentration, chemical and mineralogical composition and derived optical parameters of the boundary layer aerosol at Tinfou, Morocco, during SAMUM 2006, Tellus, 61B, 32ï 50, 2009.

Karner, D. B., Marra, F., and Renne, P. R.: The history of the Monti Sabatini and Alban Hills volcanoes: groundwork for assessing volcanic-tectonic hazards for Rome, J. Volcanol. Geoth. Res., vol. 107, 185-219, 2001.

Kassianov, E. I., Flynn, C. J., Ackerman, T. P., and Barnard, J. C.: Aerosol single-scattering albedo and asymmetry parameter from MFRSR observations during the ARM Aerosol IOP 2003, Atmos. Chem. Phys., 7, 3341-3351, doi:10.5194/acp-7-3341-2007, 2007.

Kaufman, Y. J., Tanre, D., Gordon, H. R., et al.: Passive remote sensing of tropospheric aerosol and atmospheric correction for the aerosol effect, J. Geophys. Res., 102, 16,815ï 16,830, 1997.

Kim, H. K., Hwang, H. J., Un Ro, C.: Single-particle characterization of soil samples collected at various arid areas of China, using low-Z particle electron probe X-ray microanalysis, Spectrochim. Acta, Part B, 61, 393ï 399, 2006.

Kokhanovsky, A. A.: Aerosol Optics. Light Absorption and Scattering by Particles in the Atmosphere, Springer, Germany, ISBN 978-3-540-23734-1, 2008.

Kotchenova, S. Y., Vermote, E. F., Levy, R., and Lyapustin, A.: Radiative transfer codes for atmospheric correction and aerosol retrieval: Intercomparison study, Appl. Optics, 47, 2215ï 2226, doi:10.1364/AO.47.002215, 2008.

Krueger, B. J., Grassian, V. H., Cowin, J. P., Laskin, A.: Heterogeneous chemistry of individual mineral dust particles from different dust source regions: the importance of particle mineralogy, Atmos. Environ., 38, 6253ï 6261, 2004.

Kulkarni, P., Baron, P. A., and Willeke, K.: Fundamentals of single particle transport, in: Aerosol Measurement: Principles, Techniques, and Applications, 3rd Ed.: Kulkarni, P., Baron, P. A., and Willeke, K. Editors, John Wiley &Sons Ltd., U.S., chapter 8, 24-25, 2011.

Levin, Z., Ganor, E., Gladstein, V.: The effects of desert particles coated with sulfate on rain formation in the Eastern Mediterranean, J. Appl. Meteorol., 35, 1511-1523, 1996.

Liley, J. B.: Fitting Size Distributions to Optical Particle Counter Data, Aerosol Sci. Tech., 17, 2, 84-92, 1992.

Mahowald, N., Albani, S., Kok, J. F., Engelstaeder, S., Scanza, R., Ward, D. S., Flanner, M. G.: The size distribution of desert dust aerosols and its impact on the Earth system, Aeolian Res., 15, 53ï 71, 2014.

Meloni, D., Di Sarra, A., Pace, G., Monteleone, F.: Aerosol optical properties at Lampedusa (Central Mediterranean). 2. Determination of single scattering albedo at two wavelengths for different aerosol types, Atmos. Chem. Phys., 6, 715ï 727, 2006.

Moore, D. M. and Reynolds, R. C.: X-ray diffraction and the identification and analysis of clay minerals, Oxford University Press, Oxford, 1997.

Moreno, T., Amato, F., Querol, X., Alastuey, A., Elvira, J., Gibbons, W.: Bedrock controls on the mineralogy and chemistry of PM10 extracted from Australian desert sediments, Environ. Geol., 57, 411ï 420, doi:10.1007/s00254-008-1312-2, 2009.

Müller, T., Schladitz, A., Massling, A., Kaaden, N., Kandler, K., Wiedensohler, A.: Spectral absorption coefficients and imaginary parts of refractive indices of Saharan dust during SAMUM-1, Tellus, 61B, 79ï 95, 2009.

Newbury, D. E. and Ritchie, N. W. M.: Is Scanning Electron Microscopy/Energy Dispersive X-Ray Spectrometry (SEM/EDS) quantitative? Scanning, 35, 141ï 168, 2013.

Nickovic, S., Vukovic, A., Vujadinovic, M., Djurdjevic, V., Pejanovic, G.: Technical Note: High-resolution mineralogical database of dust-productive soils for atmospheric dust modeling, Atmos. Chem. Phys., 12, 845ï 855, 2012.

OAQPS Staff: Review of the National Ambient Air Quality Standards for Particulate Matter: Policy assessment of scientific and technical information, OAQPS Staff Paper, EPA-452/R-05-005, chapter 2, 2005.

Papayannis, A., Mamouri, R. E., Amiridis, V., Remoundaki, E., Tsaknakis, G., Kokkalis, P., Veselovskii, I., Kolgotin, A., Nenes, A., and Fountoukis, C.: Optical-microphysical properties of Saharan dust aerosols and composition relationship using a multi-wavelength Raman lidar, in situ sensors and modelling: a case study analysis, Atmos. Chem. Phys., 12, 4011ï 4032, 2012.

Peng, F. and Effler, S. W.: Suspended minerogenic particles in a reservoir: Light-scattering features from individual particle analysis, Limnol. Oceanogr., 52(1), 204ï 216, 2007.

Pentecost, A.: Travertine, Springer, U.S., chapter 7, 124, ISBN: 1-4020-3523-3, 2005.

Perrino, C., Canepari, S., Catrambone, M., Dalla Torre, S., Rantica, E., and Sargolini, T.: Influence of natural events on the concentration and composition of atmospheric particulate matter, Atmos. Environ., 43, 4766ï 4779, 2009.

Pietrodangelo, A., Salzano, R., Rantica, E., Perrino, C.: Characterisation of the local topsoil contribution to airborne particulate matter in the area of Rome (Italy). Source profiles, Atmos. Environ., 69, (2013) 1-14, 2013.

Potts, P. J.: A Handbook of Silicate Rock Analysis, Blackie, U.K., 1987.

R Core Team: R: A language and environment for statistical computing. R Foundation for Statistical Computing, Vienna, Austria, 2013. Available at: http://www.R-project.org/

Rashki, A., Eriksson, P. G., de W. Rautenbach, C. J., Kaskaoutis, D. G., Grote, W., Dykstra J.: Assessment of chemical and mineralogical characteristics of airborne dust in the Sistan region, Iran., Chemosphere, 90, 227ï 236, 2013.

Reid, J. S., Jonsson, H. H., Maring, H. B., Smirnov, A., Savoie, D. L., Cliff, S. S., Reid, E. A., Livingston, J. M., Meier, M. M., Dubovik, O., and Tsay, S. C.: Comparison of size and morphological measurements of coarse mode dust particles from Africa, J. Geophys. Res., 108, D19, 8593-, doi:10.1029/2002JD002485, 2003.

Ritz, C., and Streibig, J. C.: Nonlinear Regression in R, Springer, New York, ISBN: 978-0-387-09615-5, 2008. Rocha-Lima, A., Martins, J. V., Remer, L. A., Krotkov, N. A., Tabacniks, M. H., Ben-Ami, Y., and Artaxo, P.: Optical, microphysical and compositional properties of the Eyjafjallajökull volcanic ash, Atmos. Chem. Phys., 14, 10649ï 10661, doi:10.5194/acp-14-10649-2014, 2014.

Rudnick, R. L. and Gao, S.: Composition of the Continental Crust, in: Treatise on Geochemistry: Holland, H. D. and Turekian, K. K. Editors, Elsevier, Amsterdam, vol. 3, 1ï 64, ISBN: 978-0-08-043751-4, 2003.

Sarbas, B. and Nohl, U.: The GEOROC database as part of a growing geoinformatics network, in: Geoinformatics 2008ð Data to Knowledge, Proceedings, U.S. Geological Survey Scientific Investigations Report 2008-5172: Brady, S. R., Sinha, A. K., and Gundersen, L. C. Editors, 42-43, 2008. Available at: http://georoc.mpch-mainz.gwdg.de/georoc/Start.asp

Scheuvens, D., Schütz, L., Kandler, K., Ebert, M., Weinbruch, S.: Bulk composition of northern African dust and its source sediments - A compilation, Earth-Sci. Rev., 116, 170ï 194, 2013.

Scheuvens, D. and Kandler, K..: On Composition, Morphology, and Size Distribution of Airborne Mineral Dust, in: Mineral Dust. A Key Player in the Earth System, chapter 2, Pages 15-49. Knippertz, P. and Stuut, K. J.-B. W. Editors, Springer, U.S., ISBN: 978-94-017-8978-3, 2014.

Smith, A. J. A. and Grainger, R.G.: Does variation in mineral composition alter the short-wave light scattering properties of desert dust aerosol?, J. Quant. Spectrosc. Radiat. Transfer, 133, 235ï 243, 2014.

Sokolik, I. N. and Toon, O. B.: Incorporation of mineralogical composition into models of the radiative properties of mineral aerosol from UV to IR wavelengths, J. Geophys. Res., 104, D8, 9423-9444, 1999.

Sokolik, I. N., Winker, D. M., Bergametti, G., Gillette, A., Carmichael, G., Kaufman, Y. J., Gomes, L., Schuetz, L., Penner, J. E.: Introduction to special Sect.: Outstanding problems in quantifying the radiative impacts of mineral dust, J. Geophys. Res., 107, D15, 18,015-18,027, 2001.

Stuut, J.- B., Smalley, I., OôHara-Dhand, K.: Aeolian dust in Europe: African sources and European deposits, Quatern. Int., 198, 234ï 245, 2009.

Van Dyck, P., Storms, H., Van Grieken, R.: Automated quantitative electron microprobe analysis of particulate material, Journal de Physique, C2, suppl. au n.2, 45, 781-784, doi: 10.1051/jphyscol:19842179, 1984.

Vermote, E. F., Tanrè, D., Deuzè, Herman, M., Morcrette, J. J., and Kotchenova, S. Y.: Second simulation of a satellite signal in the solar spectrum - vector (6SV), 6S User Guide Version 3, 2006. Available at: http://6s.ltdri.org

Vermote, E. F., Tanrè, D., Deuzè, J. L., Herman, M., and Morcrette, J. J.: Second simulation of the satellite signal in the solar spectrum, 6S: An overview, IEEE T. Geosci. Remote, 35, 675ï 686, doi:10.1109/36.581987, 1997.

Viana, M., Pey, J., Querol, X., Alastuey, A., de Leeuw, F., Lükewille, A.: Natural sources of atmospheric aerosols influencing air quality across Europe, Sci. Total. Environ., 472, 825ï 833, 2014.

Wagner, R., Ajtai, T., Kandler, K., Lieke, K., Linke, C., Müller, T., Schnaiter, M., and Vragel M.: Complex refractive indices of Saharan dust samples at visible and near UV wavelengths: a laboratory study, Atmos. Chem. Phys., 12, 2491ï 2512, 2012.

WCP-112: A Preliminary Cloudless Standard Atmosphere for Radiation Computation. Geneva, World Meteorological Organization, 1986.

White, A. F. and Buss, H. L.: Natural weathering rates of silicate minerals, in: Treatise on Geochemistry, 2nd Ed., Vol 7, Pages 115-155. Holland, H. D. and Turekian, K. K. Editors, Elsevier, Amsterdam, vol. 7, 115-155, ISBN: 978-0-08-043751-4, 2014.

Wilks, D. S.: Statistical methods in the atmospheric sciences, 2nd Ed., Elsevier, Amsterdam, chapter 5, ISBN: 13:978-0-12-751966-1, 2006.

Willis, R. D., Blanchard, F. T. and Conner, T. L.: Guidelines for the Application of SEM/EDX Analytical Techniques to Particulate Matter Samples, US EPA Report n. 600/R-02/070, 2002.

Ziebold, T. O.: Precision and sensitivity in electron microprobe analysis, Anal. Chem., 39, 8, 858ï 861, 1967.

1 Table 1. Quality assessment of SEM XEDS microanalysis.

	Dust	Mineral particle	K	Na	Ca	Mg	Fe	Mn	Al	Si	Ti
Repeatability (% rsd[a])	Volcanics		10	28	14	19	12	39	6	6	29
	Road dust		35	43	33	23	33	34	36	31	54
	Siliciclastics		15	24	10	13	17	31	11	8	56
	Travertine		17	25	2	25	21	31	14	6	54
Consistency with XRF (% æ[b] ± prop. error)	Volcanics		2.4 ± 0.1	55.4 ± 0.1	22.7 ± 0.3	-	32.2 ± 0.1	500 ± 10	15.8 ± 0.2	10.8 ± 0.1	41.4 ± 0.5
	Road dust		37.5 ± 0.3	> 100	28.2 ± 0.1	> 100	37.7 ± 0.7	> 100	22.3 ± 0.2	37.4 ± 0.2	87.6 ± 1.4
	Siliciclastics		22.2 ± 0.1	78.7 ± 2.1	39.2 ± 0.7	52.4 ± 0.3	10.8 ± 0.2	470 ± 10	2.8 ± 0.1	50.7 ± 0.2	7.8 ± 0.5
Accuracy (g cm^{-3})		Quartz	-	-	-	-	-	-	-	3.4 ± 0.02	-
		Kaersutite	0.07 ± 0.02	0.04 ± 0.03	0.24 ± 0.02	0.23 ± 0.03	0.67 ± 0.01	0.02 ± 0.01	0.49 ± 0.02	1.12 ± 0.02	0.11 ± 0.02

	Calcite	-	-	4.1 ± 0.02	-	-	-	-	-	-
Accuracy (% æ[c] ± prop. error)	Quartz	-	-	-	-	-	-	-	28 ± 0.4	-
	Kaersutite	37.3 ± 0.6	94.1 ± 18.3	47.4 ± 1.5	38.6 ± 0.3	28.6 ± 0.2	61.5 ± 1.8	28 ± 0.3	6.4 ± 0.3	40 ± 2
	Calcite	-	-	52 ± 1	-	-	-	-	-	-

a. % relative standard deviation

b. % æ : absolute percent difference between elemental composition determined by SEM XEDS and elemental composition of same local dust determined by ED-XRF (Pietrodangelo et al., 2013). Prop. err.: propagated error.

c. % æ : absolute percent difference between the element %wt in the mineral particle and the element %wt in the bulk standard mineral (EDAX Inc.). Prop. err.: propagated error.

Table 2. Average mineral composition (% wt) of dust samples by XRD analysis.

	Volcanic rocks	Siliciclastic rocks	Marlstones	Road dust (Volcanics)	Road dust (Travertine)	Travertine*
Phyllosilicates	57	52	26	7	-	-
Tectosilicates	18	6	0.7	8.7	6	-
Inosilicates	26	-	1.5	22.7	10.2	-
Quartz	4	11	4	1.3	3	-
Calcite	-	31	68	60.3	81	> 90

* After Pentecost (2005)

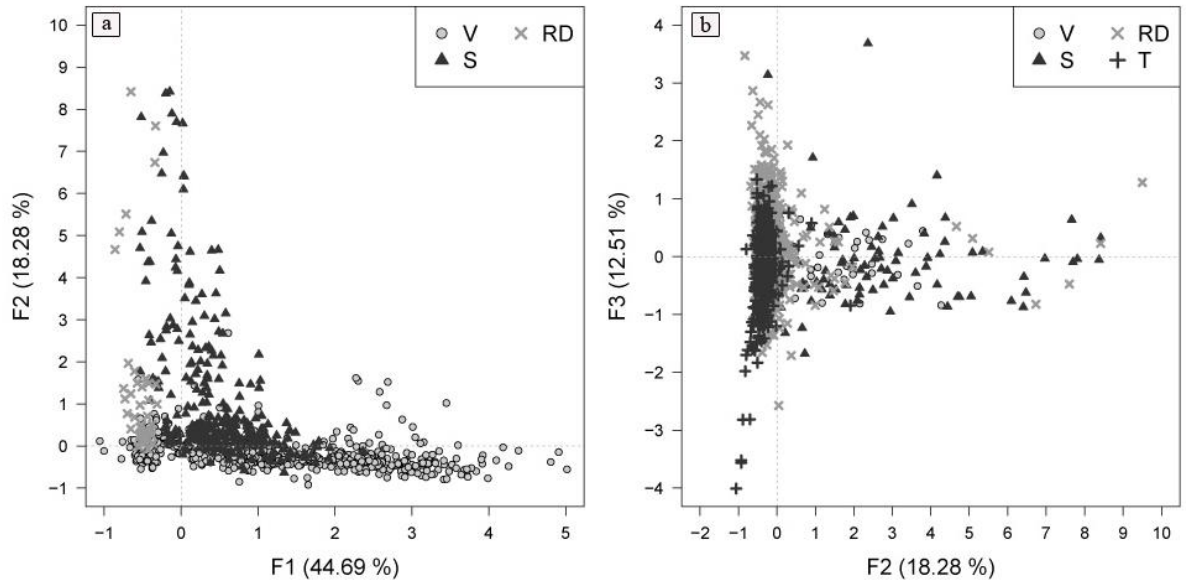

Figure 1. PCA of elemental ratios calculated on individual dust particles composition: score plots of factors (F1, F2, F3) with eigenvalue higher than unity. V: volcanics; S: siliciclastics; RD: road dust; T: travertine.

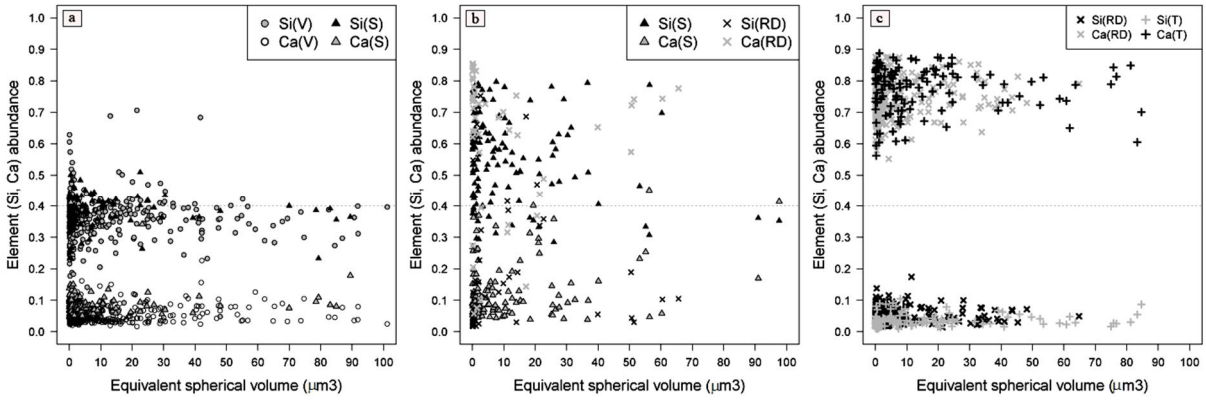

Figure 2. Ca and Si abundances of particles with highest PCA score in F1 (a), F2 (b), or F3 (c), plotted versus the particle equivalent spherical volume.

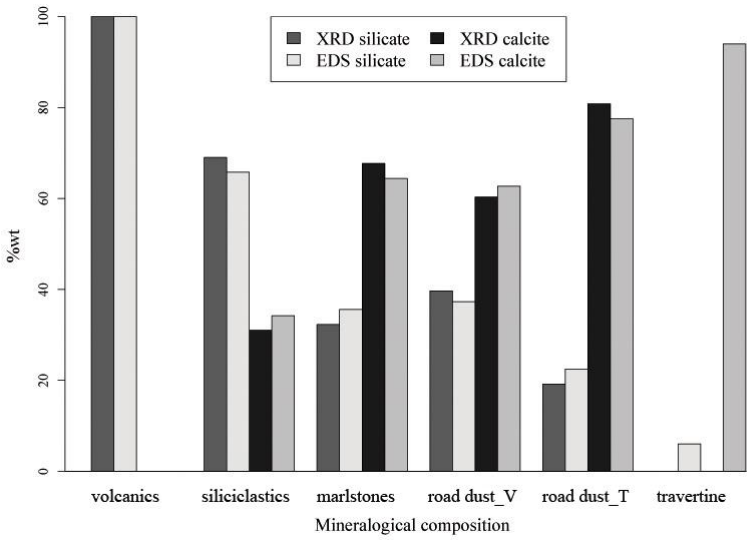

Figure 3. Total silicate (including quartz) and calcite amounts (%wt) of dust samples, obtained by X-ray diffraction bulk analysis and SEM XEDS particle microanalysis.

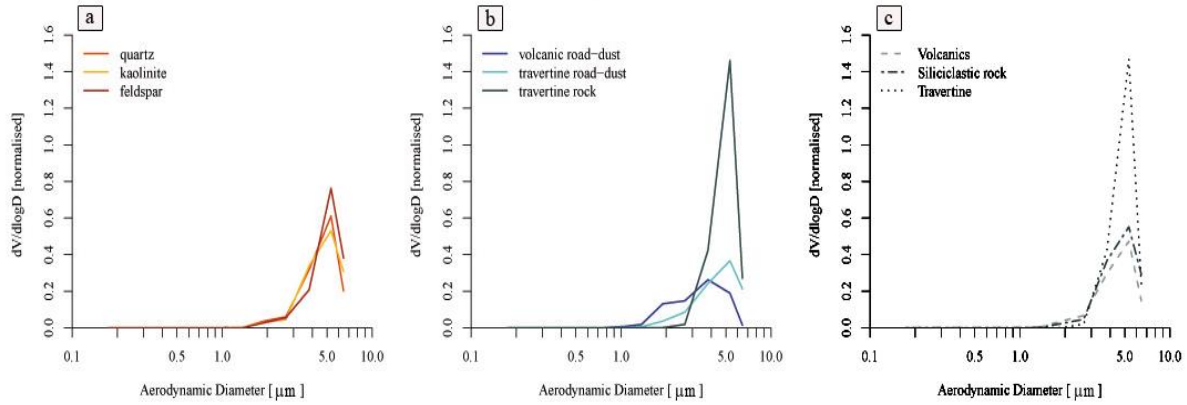

Figure 4. Normalised volume size distributions of most abundant silicates (a), calcite (b), and local dust types (c) in the PM_{10} fraction. Calcite is differentiated by natural (travertine) or anthropic (road dust) origin.

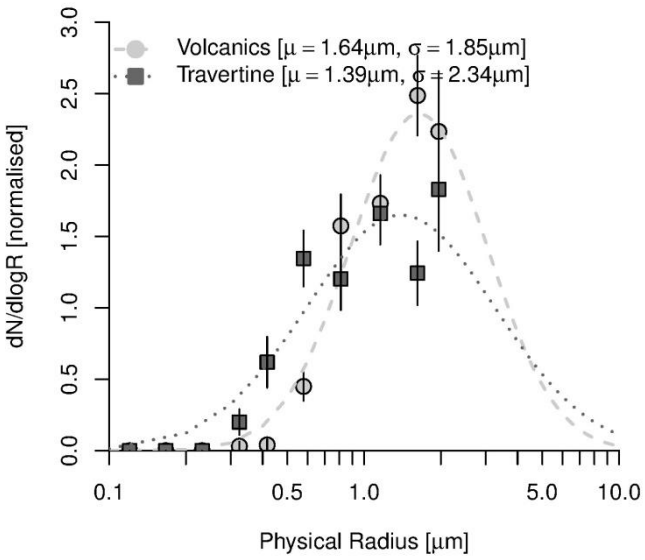

Figure 5. Probability density function fitted to log-normal distribution of the volcanics and travertine PM_{10} dust. Error bars represent uncertainties of bin weight.

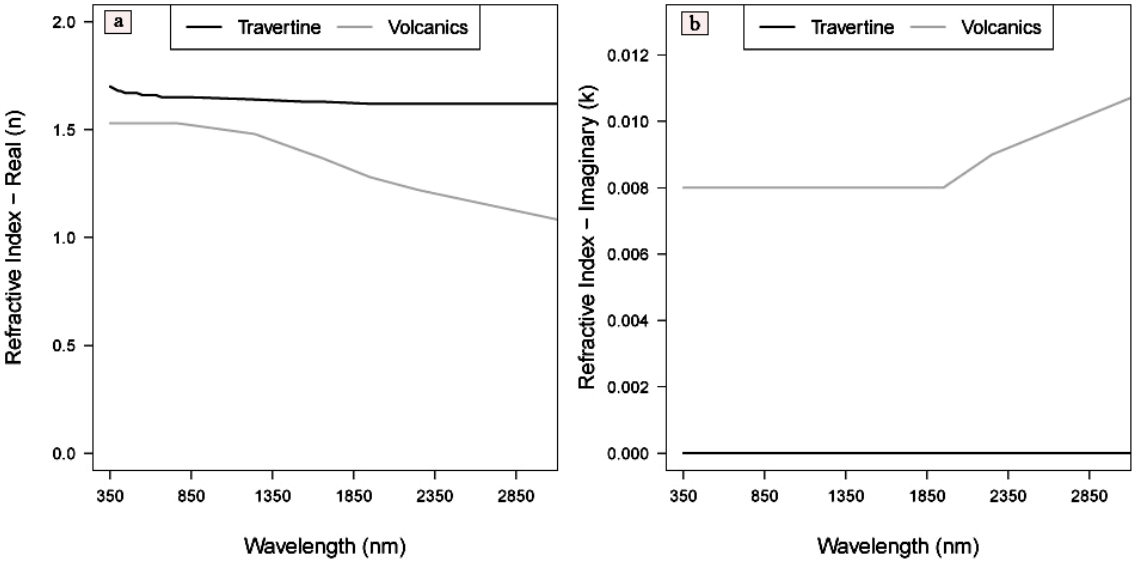

Figure 6. Real (a) and imaginary (b) part of refractive index of the volcanics and travertine PM_{10} dust.

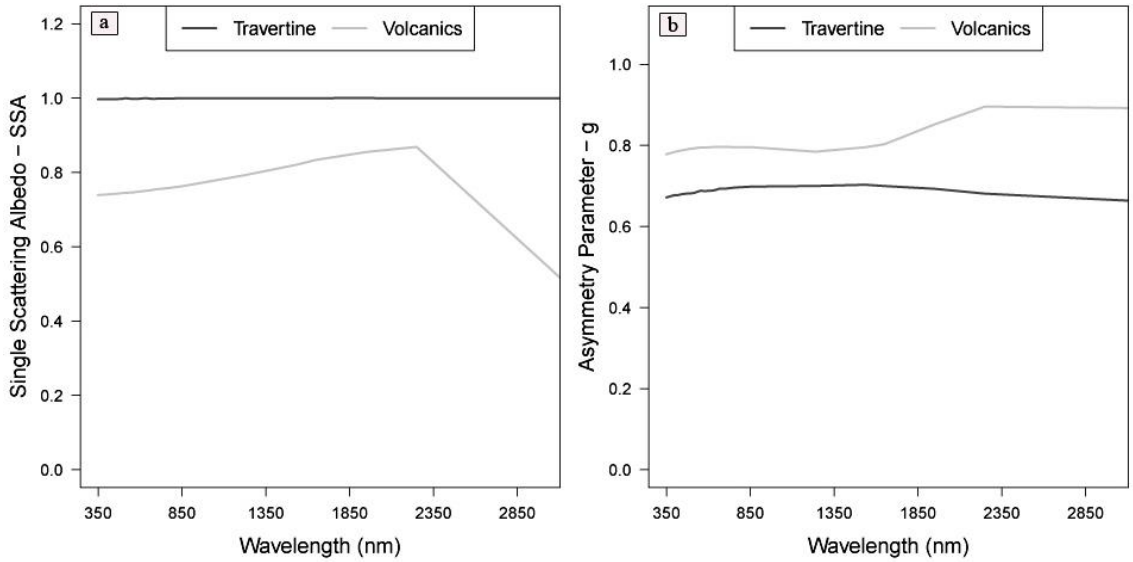

Figure 7. Single scattering albedo (a) and asymmetry parameter (b) of the volcanics and travertine PM_{10} dust.

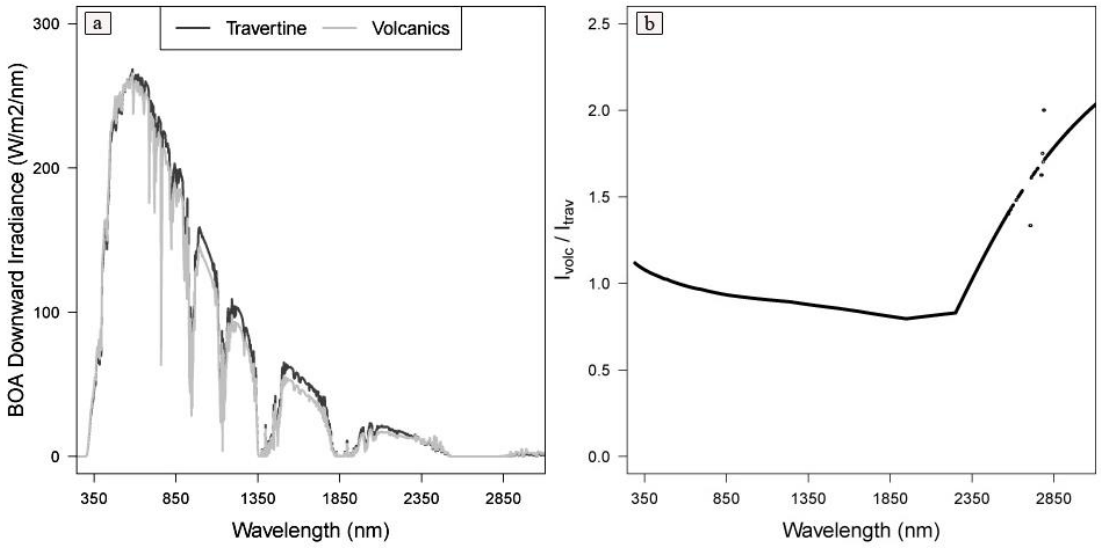

Figure 8. BOA downward solar irradiance (a) of an atmosphere composed by only volcanics, or travertine, PM_{10} dust, and volcanics to travertine irradiance ratio (b).

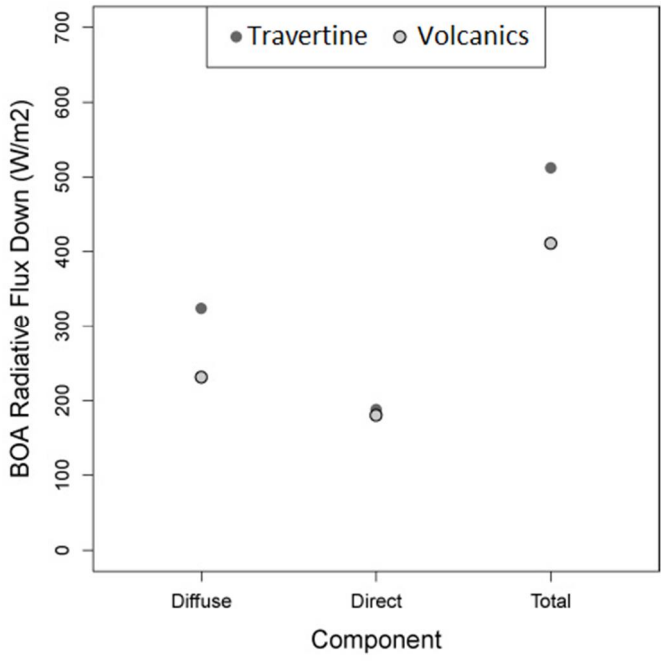

Figure 9. Diffuse, direct and total BOA downward radiative flux (W m^{-2}) over the 250 ï 4000 nm spectral domain, simulated by the 6SV code.